Influence of Pvd Deposition Mode on the Quality and Integrity of CrAlN Thin Films: A Study of Magnetron Sputtering Processes on Stationary and Rotating Substrates

Brahim TLILI , Mohamed NASSER * , Hichem GUIZENI , Alex MONTAGNE

Posted Date: 10 July 2023

doi: 10.20944/preprints202307.0562.v1

Keywords: CrAlN; corrosion; friction; microstructure; bias voltage

Article

Influence of PVD Deposition Mode on the Quality and Integrity of CrAlN Thin Films: A study of Magnetron Sputtering Processes on Stationary and Rotating Substrates

Ibrahim Tlili [1,2], Mohamed Nasser [1,2,3,*], Hichem Guizeni [1,3] and Alex Montagne [2]

[1] University of Tunis, El-Manar, National Engineering School of Tunis (LR-MAI), ENIT, BP 37 le BELVEDERE 1002 Tunis, Tunisia; tlilii_brahim@yahoo.fr (I.T.); mohamed.bennasser@kef.r-iset.tn (M.N.)

[2] Arts & Métiers ParisTech; Laboratory of Mechanics, Surfaces and Materials Processing (MSMP), 8, boulevard Louis XIV, 59046 Lille, France; alex.montagne@uphf.fr

[3.] General Directorate of Technological Studies, DGET, Higher Institute of Technological Studies of Kef (ISET-Kef), DGM-Department, Boulifa University Campus, 7100 Kef, Tunisia; guizanihichem@yahoo.fr

* Correspondence: mohamed.bennasser@kef.r-iset.tn

Abstract: The development and qualification of CrAlN coatings deposited by DC magnetron sputtering offer new industrial solutions to increase the lifecycle of material forming tools (machining and shaping). This study focuses on the selection and optimization of deposition modes for CrAlN layers to be deposited on a 90CrMoV8 tool steel substrate. The adopted methodology aims to optimize the deposition conditions to meet the customer's requirement of a CrAlN coating thickness of approximately 2-3 µm for use in a hot forming process. Different polarizations using two Al and Cr targets, with both stationary and rotating substrate modes during deposition, were tested and evaluated. Characterizations of the CrAlN coating layers (microhardness, residual stress, structures) and performance in service (wear, friction, adhesion, corrosion) were chosen as selection criteria for a particular coating mode. The aluminum content plays a crucial role in the tribological and mechanical behavior of CrAlN layers. Corrosion resistance is more sensitive to the aluminum content for the stationary deposition mode. As a result, the rotating mode provides higher adhesion (+100%) and less wear (-60%) compared to the stationary mode. Therefore, depending on the likely performance in service, either a stationary or rotating mode could be applied for coating the functional surfaces of hot forming tools.

Keywords: CrAlN; corrosion; friction; microstructure; bias voltage

1. Introduction

The needs of the cutting industry, which requires tools with excellent wear resistance, have led, for the last decades, to the development of thin layers of transition metal nitrides (TiN, TiAlN, CrN, CrAlN…) deposited by a Physical Vapor Deposition (PVD) process. Given the extreme conditions to which they are subjected, these thin films must have several specific characteristics, on the one hand to overcome the wear and corrosion of the tool material and on the other hand to guarantee good roughness of the machined part. Hardness and optimized tribological properties are the first to consider, given the potential application of these layers in the field of machining. In addition, they must exhibit good resistance to hot oxidation due to the rise in temperature concomitant with friction. Lastly, they must constitute an effective means of combating the corrosion of the substrate, for example in the case of possible lubricant attacks or during storage in an industrial atmosphere. TiN and CrN monolayer coatings have thus been widely studied over the past ten years and have been used in several applications, particularly in the field of milling for their exceptional mechanical properties. In their study, Chim and al. [1] proved that Cr-based coatings (CrN and CrAlN) clearly exhibited better oxidation resistance than Ti-based coatings (TiN and TiAlN). As a result, the oxidation process of the CrAlN layer is triggered at a slow speed. After heat treatment (annealing at 1000 ° C), only about 19% Oxygen is present and the CrAlN film remains intact.

 doi:10.20944/preprints202307.0562.v1

Chromium nitride (CrN) is widely used to increase the durability of cutting tools. This binary coating is characterized by a good tribo-corrosion behavior accompanied by a high resistance to oxidation [1,2]. Nevertheless, it has weaknesses, such as its fragility and high thermal properties [3]. To improve this coating, several studies have been performed using different protocols and conditions with analysis of their impact on the performance of the resulting thin films [4]. They developed CrN coatings under different deposition temperatures using low arc deposition technology. They showed that the tribological behavior of CrN layers strongly depends on the temperature. Indeed, when the temperature increases from 25 to 500 °C, the coefficient of friction of the CrN layer against a bead of Si_3N_4 decreases, but when sliding against an Al_2O_3 bead, the lowest friction coefficient is obtained at 25°C and 500 °C. Aouadi et al. [5] also showed that adding the proportions of aluminum to CrN can improve the tribological and anti-corrosive properties.

Following the study conducted by Tlili et al. [6], it was shown that the CrAlN (5% Al) layer has a low thermal conductivity compared to CrN, which results in higher residual stresses. Therefore, it is known that coatings containing an aluminum proportion can in some way act as a thermal barrier, which reduces the impact of thermomechanical stresses on the active part of the cutting tool (increased durability). The CrAlN system is a cutting-edge coating technology that utilizes chromium alloy as its base material. Extensive research has been conducted to investigate its deposition temperatures, which typically exceed 400°C [7–11]. Moreover, the addition of aluminum during the synthesis process significantly impacts the structure of the resulting coatings. Despite the lack of obvious correlation between the structure and aluminum content, this relationship continues to be the subject of ongoing investigations [12–15].

Over the past twenty years, most of the elaborations of the CrAlN ternary layers have used compound targets instead of two targets [15–18], and some cases are accompanied by rotation of the sample holder. Depending on the deposition technique (one or more cathodes available, with or without sample rotation) and the applications concerned, different compositions of Cr_xAl_y-coated layers have been used to deposit CrAlN coatings [19–25]. Coating thicknesses can also be targeted to suit the intended industrial application. In several configurations, the concavities, the different orientations, the displacement of the substrate and the target affect the uniformity of the coating thickness, are at the origin of the macroscopic shadows, and affect the uniformity of the coating thickness, as recently mentioned by Evrard et al. [26]. Furthermore, the effect of substrate rotation on the microstructure of the coatings has been studied and discussed in detail in studies conducted by Kadam et al. [27]. The authors showed that coating on a stationary substrate has dense and fine-grained growth behavior compared to coating on a rotating substrate.

Therefore, the aim of the present work is to identify the causes of the chemical composition change in CrAlN coatings synthesized with the substrate rotation in a new deposition technique. For this purpose, we involve the scanning transmission electron microscopy (STEM) and Energy-Dispersive Spectroscopy (EDS analysis) to study the effect of the substrate rotation on the structural and compositional evolution at the nanometer scale. We also provide a tribological and anti-corrosive behavior study of CrAlN layers.

2. Experimental details

2.1. Substrates

CrAlN films were developed firstly on stainless steel samples (90MnCrV8) of square shape with the following dimensions (20 × 20 mm^2 and 5 mm thick) and secondly on mirror polished silicon plates (100) with an area of 10 x 10 mm^2 and a thickness of ≈ 380 µm. The surface roughness of steel samples is Ra of about 0.08 µm and Rt of around 1 µm, yielding roughness like that of industrial tools. Prior to deposition, all substrates were ultrasonically cleaned with acetone and ethanol for 5 min each and then dried with compressed air. The chemical compositions in addition elements of the Mn steel substrate (90MnCrV8) are provided in Table 1.

Preprints (www.preprints.org) | NOT PEER-REVIEWED | Posted: 10 July 2023 doi:10.20944/preprints202307.0562.v1

Table 1. Chemical composition of 90MnCrV8 steel.

Chemical elements	C	Mo	V	Si	Mn	Cr	S
% Wt	0.89	1.5	0.6	1.3	0.4	5.8	0.02

2.2. Coating deposition technique

The CrAlN coatings were deposited by the reactive DC magnetron sputtering technique (KENOSISTEC-KS40V). Figure 1 shows the interior of the enclosure and the machine components. It consists of two parts: the spray system and the control panel. This projection system consists of a vertical batch in which the substrates to be coated are placed inside the enclosure. The assembly is placed on a carousel equipped with a planetary system in multiple rotations, thus transporting the substrates in front of the magnetron cathodes (vertical orientation with respect to the walls of the chamber). Note that the carousel can rotate around a central vertical axis. It consists of eight substrate carriers each has its own rotation.

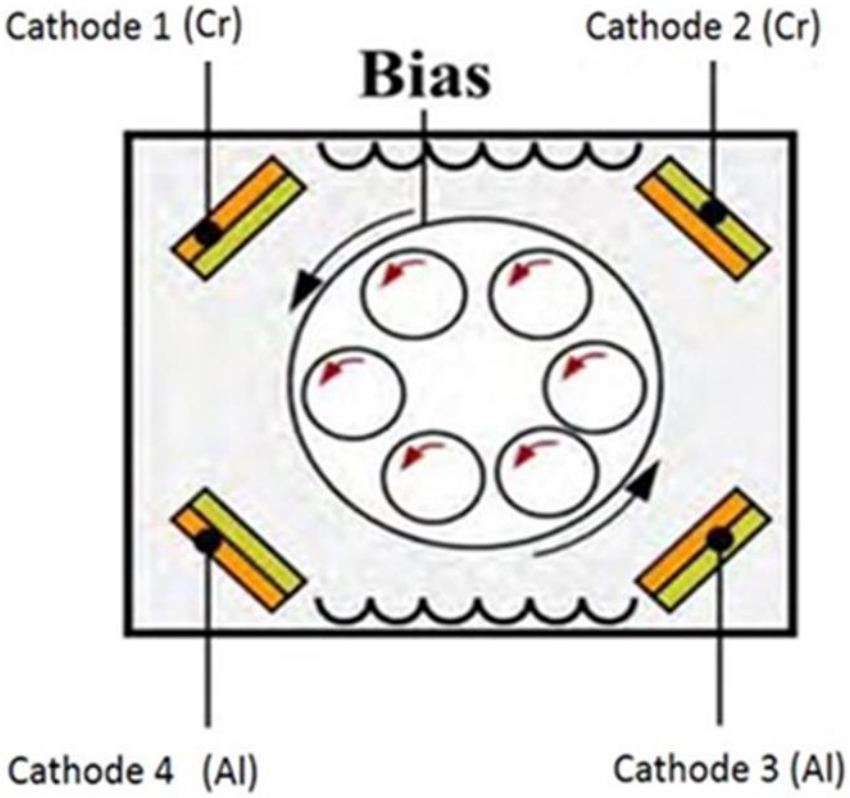

Figure 1. "KENOSISTEC" machine, model KS40V: the schematic of the coating deposition setup (top view).

The used targets are of various types [pure Cr (99.995%) and Al (99.999%) targets were used] but of identical dimensions: diameter 200 mm and thickness 6 mm. An electric motor allows the substrate holder to rotate at a speed of 14 tr/min. This substrate holder consists of a disc of 610 mm in diameter. The maximum distance in the enclosure between the target and the substrate (Dc-s max) is approximately 180 mm. In magnetron cathode sputtering, the flux is directive. For any given material, the deposition speed is a function of the distance between the target and the substrate. When this distance exceeds the average erosion diameter of the target, the deposition rate is maximum in the axis of the target. The more we increase the voltage, the more atoms we eject and the greater the directional effect. For our tests, the substrates were placed at approximately 80 mm from the center of the sample holder. This position corresponds to the location where the distance between the substrate and the target center is the smallest during their passage face to face. It is generally accepted that the minimum speed of rotation of the substrate holder follows the following relationship [28]:

Preprints (www.preprints.org) | NOT PEER-REVIEWED | Posted: 10 July 2023 doi:10.20944/preprints202307.0562.v1

$$Vt < 1\ nm \quad (1)$$

$$t = \frac{l}{2\pi\omega r} \quad (2)$$

with:

V: instantaneous deposition speed (nm.s^{-1})

t: time of passage in front of the target (s)

l: Target width (cm)

r: radius of the substrate holder (cm)

w: Speed of rotation of the substrate holder (turns.s^{-1})

Thus, the value of the speed of rotation of the substrate is of the order of 3 rpm. It is an average value conditioned by the deposition rates of the Cr and Al targets. This makes it possible to obtain a great uniformity with the best properties: physicochemical, anti-corrosive and tribological. To comprehensively evaluate CrAlN$_R$ coatings, it is imperative to analyze their microstructure, hardness, and wear resistance, particularly when prepared by a deposition system that utilizes double rotation of the substrate. The scientific literature highlights the effectiveness of these types of coatings in resisting crack propagation and exhibiting strong adhesion to the substrate. Moreover, coatings prepared through rotation demonstrate a highly uniform columnar microstructure, as well as exceptional homogeneity in both their thickness and structure [29].

Before deposition, all the substrates were ultrasonically cleaned with ethanol. The targets and the samples were then etched for 5 min in an Ar plasma by RF and DC (−1000 V) discharges, respectively. The temperature of the substrate during polarization is 300 ° C. Before the deposition, the chamber was heated at 300 °C for 7 h. During the deposition, the working pressure was set at 4 µbar. The Ar and N_2 flow rates were 80 and 20 sccm, respectively. The chromium and aluminum targets having a dimension of 406.4×127 mm^2 are used to produce the CrAlN coating.

To study the impact of the substrate rotation on the physicochemical, tribological and mechanical properties of the coatings, it is therefore necessary to develop the CrAlN films according to two methods.

1- ***CrAlN$_S$***: Targets and substrates are stationary.

2- ***CrAlN$_R$***: Rotating substrates (around their axis and around the central axis).

Table 2a,b, summarize the CrAlN deposition conditions for the two production methods (i.e., with and without rotation).

We studied the variation of parameters such as the target voltage and the power of the Al and Cr targets. But the other parameters such as the gas proportion, the operating pressure and deposition time are invariable. These values have been optimized in previous works [5]. Therefore, our study focuses only on the variation of generator power (which directly impacts the bias voltage of Cr and Al targets). It is important to accentuate that the objective of this publication is to optimize the deposition conditions for each mode. The aim is to evaluate the characteristics and durability of these thin coatings prepared using different stationary and rotational modes. The different layers of stationary or rotational coatings are to be deposited on a 90CrMnV8 substrate to make it suitable for use in the fabrication of hot forging tools. Depending on the priority order of service requirements (corrosion, fatigue, wear, etc.), the choice of one deposition mode over the other can be justified while meeting the requirement of a 2-3 µm coating thickness necessary for the targeted industrial use.

Preprints (www.preprints.org) | NOT PEER-REVIEWED | Posted: 10 July 2023 doi:10.20944/preprints202307.0562.v1

Table 2. Deposition conditions for CrAlN coatings in stationary (**CrAlNs**) and rotary (**CrAlNR**) modes.

Coatings	Target bias voltage (-V)		Gas proportion		Working pressure (µbar)	Power of Targets (w)		Deposition time [min]	Output target Thickness 2-3 [µm]
	Cr	Al	%Ar	%N_2		Cr	Al		
		0				500	0		2
		300				500	100		2.1
		500				500	250		2.5
CrAlNs	900	700	70	30	4	500	350	120	2.7
		900				525	450		3
		900				550	550		2.1
		900				575	550		2
		220					500		2.2
		225					1000		2.3
CrAlNR	375	236	70	30	5	1500	1500	120	2.5
		243					2200		2.7
		256					2800		2.9

2.3. Characterizations

The mechanical and microstructural characterization of CrAlN coatings is established in terms of crystallography, surface topography, nanohardness, roughness, and residual stresses. Scanning electron microscopy (SEM) observations coupled with atomic force microscopy (AFM) analyses allowed for a structural characterization of the coating layers. The crystallite size was determined using Scherrer's formulas [30]. Analytical modeling based on Stoney's equations [13] provided a realistic evaluation of residual stresses, while nanoindentation techniques were utilized [31–33] to identify the hardness and stiffness of the CrAlN layers. This enabled the consideration of the substrate effect on the nanoindentation results to extract the true hardness and stiffness properties of the CrAlN coating layers.

The evaluation of the performance of the coating layers in service is established through wear and corrosion tests. Wear tests are conducted by rotating an alumina ball (diameter 6 mm) against a disc under a fixed normal load of 2 N, a sliding speed of 3 cm/s, and a total sliding distance of 100 m, followed by an instantaneous recording of the coefficient of friction. The chemical analysis of wear traces on the contacting antagonists is determined by energy-dispersive X-ray spectroscopy (EDS) analysis. Corrosion tests were performed in a corrosive medium using a 3% aqueous solution of NaCl. Polarization curves are developed, and the potential is swept within the activation potential range [Eocp ± 250 mV].

3. Results and discussion

3.1. Chemical composition and microstructure of layers

3.1.1. EDS analysis of the CrAlN layers

We have plotted the evolution of the chemical composition of the CrAlN layer as a function of the polarization voltage of the aluminum target (Figure 2) with an average uncertainty margin of 0.1%. It is observed that logically, the chromium content decreases while the aluminum content increases. Following the results obtained (Figure 2-a), it turns out that it is the variation in the voltage on the chromium target which is the predominant parameter. This is because the sputtering rate of chromium is higher than that of aluminum, as confirmed by the concentration of Al which remains higher than that of Al for the same voltage applied to the two targets (-900 V). On the other hand, by increasing the power applied to the aluminum and chromium targets (Figure 2a-b) to 2800 W and

Preprints (www.preprints.org) | NOT PEER-REVIEWED | Posted: 10 July 2023 doi:10.20944/preprints202307.0562.v1

1500W, respectively, we obtain a comparable sputtering rate on the two targets (Cr and Al), and thus almost identical percentages of the two elements in the CrAlN layer. Indeed, the sputtering yield deposition rate of Al is 1.08 atoms / ions and that of Cr is 1.36 atoms/ions [34–37]. The nitrogen percentage decreases slightly with the increasing power of the Al target up to 2800 W, indicating a slight substoichiometry for aluminum rich films. Similar results have been shown by Romero et al. [38] and López et al. [39].

Moreover, the overall content (Cr +Al) of the metallic elements remains substantially constant, because of the nitrogen content in the films. However, we note that the constant sensitivity is more regulated on CrAlN$_R$ than on CrAlN$_S$ films, which proves the impact of the rotation of the substrate on the homogeneity of the film. The results confirm that the structure of the CrAlN films synthesized in this work forms a solid solution allowing the substitution of Cr atoms by Al atoms because the radius of the covalent bond of Al (about 0.125 nm) is smaller than its counterpart of Cr (about 0.139 nm). The positions of Al atoms in the basic unit cell of the microstructure of a Cr lattice provide greater homogeneity to the CrAlN$_R$ layer. Due to the deposition temperature and deposition conditions meeting the thickness constraint of 2-3 μm, the nitrogen (N) atoms and their connection with the substrate atoms appear to be negligible. However, to achieve constructive results for further studies, investigations into the Cr-Al-N ternary phase diagram and the interactions with the substrate at the interface are being considered for both stationary and rotational modes.

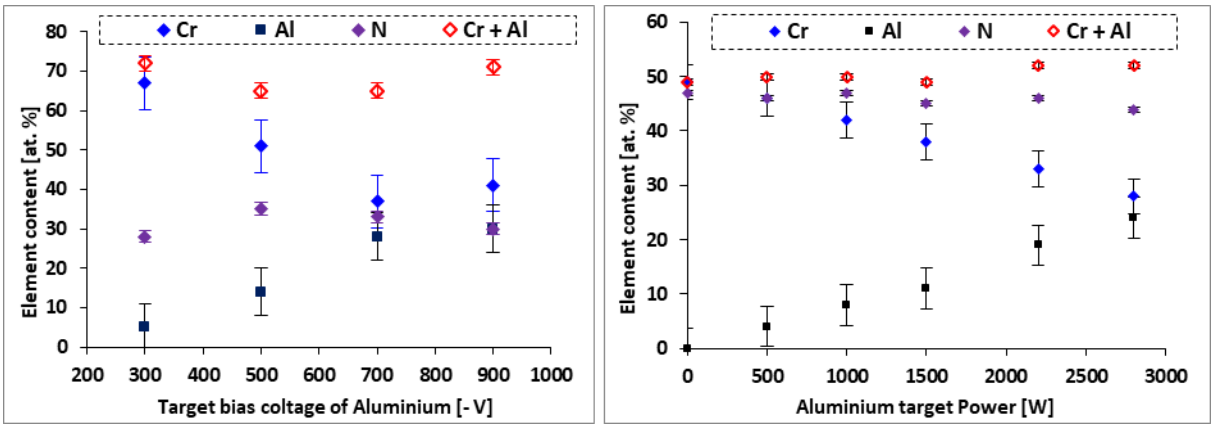

Figure 2. EDS results of CrAlN coatings: (**a**) Targets and substrates are stationary (CrAlN$_S$), under increasing the bias voltage of the Al target, and (**b**) two-fold substrate rotation (CrAlN$_R$), under increasing the power of the Al target.

In rotation mode, the impact of density and plasma fluxes on the incorporation of reactive species has been investigated in deposition experiments, and the preferred incorporation of Nitrogen (N) occurs when the growing coating surface faces the ion source. Thus, the growing surface is positioned in front of a region of high plasma density and characterized by large fluxes of film-forming species. The preferred incorporation of N takes place in a region of low plasma density where small fluxes are present. As the growing surface approaches the ion source under the effect of the rotational movement, low modulations in composition are observed (Figure 3). This is caused by the rotation of the substrate since the growing coating surface is periodically exposed to regions of high plasma density and large fluxes of film-forming species and regions of low plasma density and small fluxes. These findings are highly relevant to all reactive industrial processes of plasma-assisted PVD coatings using substrate rotation.

Preprints (www.preprints.org) | NOT PEER-REVIEWED | Posted: 10 July 2023 doi:10.20944/preprints202307.0562.v1

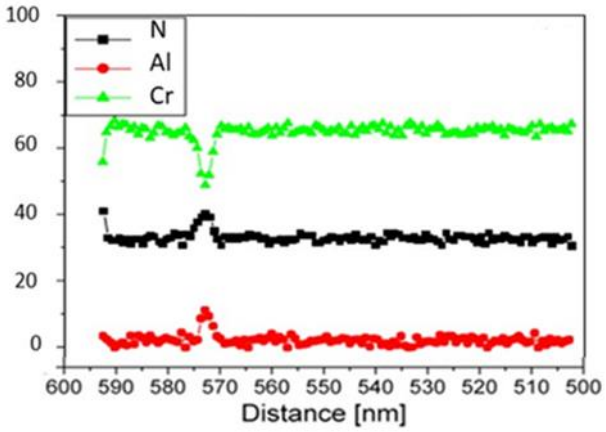

Figure 3. Chemical composition profile along the coating growth direction of **CrAlN$_R$** synthesized with two-fold substrate rotation at a reduced carousel rotation speed of approximately 3 rpm, with power = 2200 W of the Al target.

Nitrogen (N) is easily incorporated in the zone under high plasma density and relevant flux of film-forming species (substrate in front of the ionization source) [12]. It is logical to estimate that the reactions of non-metallic species in areas with high and low plasma densities are significantly different. CrAlN films are synthesized in abundance of nitrogen and in regions subject to high plasma density. Hence, the activation of nitrogen can build up by N^{2+} and N^{+} [12]. However, for the growth conditions employed in our study, the modulations seem sensitive to variations caused by the rotation of the substrate, in the density of the plasma and related to changes in the flux of film-forming species. It is reasonable to think that the modulations of the different chemical species have implications on the performance of the coating (homogeneous, mechanical and tribological properties…). Therefore, these results are very relevant to the correct conduct of industrial processes of working under vacuum (plasma) with a mixture of reactive gases and under a rotation/stationary substrate. This is because the active surface (growth surface) will regularly encounter regions with fluctuating plasma density (high and low) that feature varying fluxes (significant and minor). As a result, the modulations of the chemical composition identified in this study at the nanoscale are influenced by periodic variations in plasma density and the fluxes of the film-forming species. These variations are induced by the rotation of the substrate. In addition, chemical modulations can be expected to occur in all plasma-assisted reactive industrial PVD processes using substrate rotation and may have drastic implications on the properties of the functional coatings. This modulation behavior is attenuated under the effect of the optimization of the speed values (Eq. 1 and Eq. 2). This relationship makes it possible to reduce the amplitude and the period of the modulations, and therefore the homogeneous growth of the CrAlN layer.

3.1.2. Morphology of the CrAlN layers

Transmission electron microscopy is a very precise technique which gives clearer information on the growth mode of thin films, their morphology, and their structure (Figure 4a). To better compare, we chose the sample coated with 5% Aluminum, which exhibits better tribological performance, as shown in the work of Tlili et al. [6]. We noticed that the layer is nanostructured over 25 nm at the substrate/deposition interface, with a period of 3 to 3.5 nm. Growth then continues with a columnar structure in the form of grains surrounded by an amorphous matrix (Figure 4a). These observations correlate with the X-Ray Diffraction DRX analyzes (Figure 6) which showed a large peak for the CrAlN layer (5% Al) proving that it is amorphous. Wang et al. [36] have shown that the addition of Al allows the formation of amorphous/nanocrystalline nanocomposites and observed the presence of several nanocrystalline particles, in the form of super-lattices, of more than 20 nm in grain size and 0.20 nm period, surrounded by an amorphous structure. This crystalline phase is attributed to CrN (111) while Al is implanted in the amorphous phase. Further away from the substrate/coating interface, the CrAlN layer has a two-phase structure, formed of CrN and AlN. This phenomenon

Preprints (www.preprints.org) | NOT PEER-REVIEWED | Posted: 10 July 2023 doi:10.20944/preprints202307.0562.v1

attests that the doping of Al in the CrN matrix strongly promotes the development of a mixed amorphous /crystalline nanocomposite microstructure. Our results are in line with those of Bobzin et al. [22] where only a crystal phase attributed to a metastable structure of CrAlN (200) is observed.

Figure 4b represents an electron diffraction image of the CrAlNs layer (5% Al). The rings obtained are discontinuous which confirms the inhomogeneity of the structure of the obtained film. Two inter-reticular distances could be measured, the first of 2.45 nm and the second of 2.04 nm. It is difficult to identify the first distance, while the second is measured according to Bobzin et al. [22], relating to a new cubic structure of (Cr,Al)N having an inter-planar distance of 2.03 nm. Bobzin et al. [22] carried out a Gaussian study of the diffraction peak obtained for a CrAlN layer of 29.6% Cr, 12.5% Al, 54.5% nitrogen and traces of carbon and oxygen. They showed that the DRX peak of this new phase is at an angle of 43 °, between that of Cr_2N (111) and CrN (200), using a copper anode ($\lambda_{Cu\ K\alpha}$ = 325 nm). The comparison of the results obtained by transmission electron microscopy (TEM) (Figure 4b) with those of DRX (Figure 5), leads us to believe that the layer of CrAlN at 5% Al is a multiphase composite (Cr_2N, CrN and AlN).

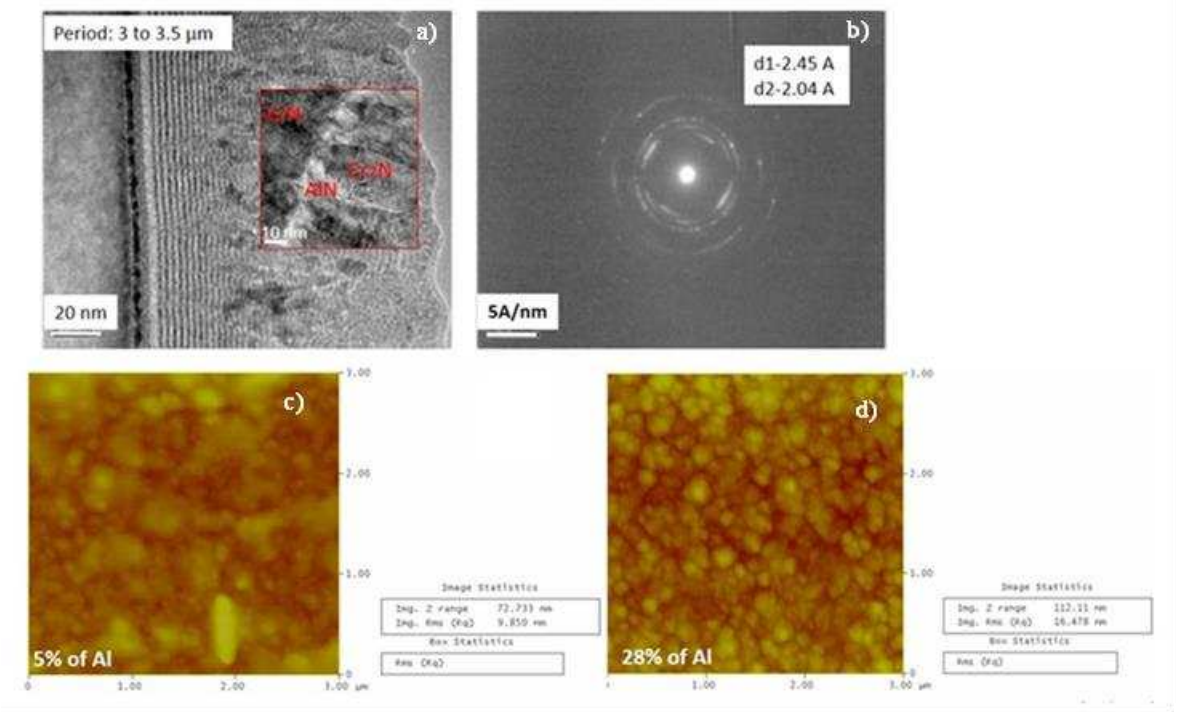

Figure 4. Morphology of CrAlNs film: **a)** TEM image at 5% of Al, **b)** Electron diffraction spectrum at 5% of Al, and **c)** Three-dimensional AFM surface morphologies of CrAlNs coatings at 5%, and **d)** for 28% of Al.

The surface topography, given by atomic force microscopy (AFM) in Figure 4, is globally uniform with some dimes and tiny craters spread all over the area (Figure 4c). The dimensional measurements show that the domes have an average diameter (dm) around 30 nm, the craters have a maximum depth (P_{max}) of 73 nm, and the roughness (RMS) is about 10nm (CrAlNs at 5% Al). The dimensions of the CrAlN layers increase with the bias voltage (or Al%), which is justified on the same coating at 28% Al, with dm measuring approximately 55 nm, and P_{max} is of the order of 112 nm. The root-mean-square (RMS) surface roughness values of the CrAlN coating with the proportions of aluminum are quite different. Apparently, the surface roughness is proportional to the ratio of aluminum. The CrAlN coating is very smooth with an RMS value of about 9.8 nm for 5% Al, while the surface roughness increases to 16.5 nm for 28% Al (Figure 4c).

Consequently, the particle size of the CrAiNs film increases as the proportion of aluminum increases (about 10 nm for 5% Al and 20 nm for 28% Al). This change in particle size is accompanied by a phase change in the layer and an overall alteration in the coating's structure. These findings align

 doi:10.20944/preprints202307.0562.v1

with the general observations of sputter deposition, wherein the deposition rate increases as the substrate-target distance decreases [36].

In the case of stationary substrates, the substrate-target distance was the shortest and kept constant, and therefore, the substrates are more exposed to the denser and constant flux of adatoms from the sputtering target. Further, during the rotation of the substrate, the substrate-target distance varies from 70 mm to 180 mm with a weaker ion cloud of the flow of adatoms, and the deposition rate decreases. Thus, the structure is columnar with low density (Figure 5a). In addition, the shadow effect is maximum in the case of a rotating substrate, which promotes the porosity of the $CrAlN_R$ film (Figure 5b). For the lowest percentage of Al (3.5%), AFM analysis shows small grains covering the entire surface of the substrate. These particles of tiny craters and domes of different sizes are distributed randomly. By doping more Al (24%), we observe that domes and tiny craters still exist all over the area, but the surface is a little denser, and the grain size is higher. This coincides with Figure 4b and with other papers [6]. This alteration in the film surface can be attributed to the high ionization rate and ion projection enhanced by the high bias voltage applied to the substrate. Thus, the growth rate of the $CrAlN_R$ layer is very high, which results in a 3D growth on the top surface of the coating (Figure 5b).

Based on the analysis of TEM images for the ternary $CrAlN_R$ layer (Figure 5), we find that this surface layer is composed of a well-developed crystalline phase following relatively arranged grain geometries, where the grain size measures about 20 nm. In addition, we notice that the large grains of this film are superimposed on small grains of the order of a few nanometers, and on a larger scale, the crystalline grains of average size of around 5 nm (black area) are developed in the part of the amorphous structure (white area) (Figure 5c). The System Architecture Diagram (SAD) of the coating shows and specifies the presence of the diffraction peaks (111), (200) and (220) associated with a cubic phase structure centered on the face. This could be attributed to the nanocrystalline Cr-Al-N solid solution integrated in an amorphous matrix. Subsequently, the enlargement of the image of this structure (Figure 5d), shows nanoparticles distributed along an interplanar crystal spacing of 0.206 nm, which is consistent with the orientation of the typical crystal plane of CrN (111). As a result, Al is mainly present in the amorphous structure. The High-Resolution TEM (HRTEM) image of Figure 4c shows that the doping of Al in the CrN matrix strongly fosters the development of a mixed amorphous/crystalline nanocomposite micro-structure.

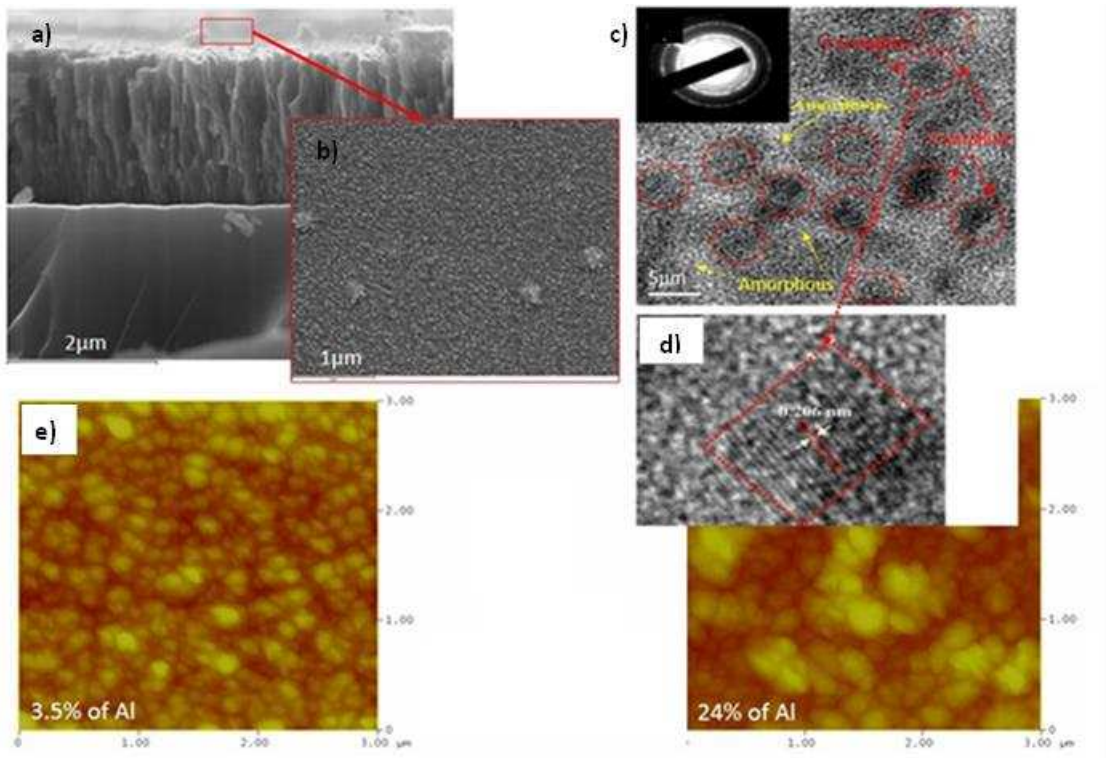

 doi:10.20944/preprints202307.0562.v1

Figure 5. Morphology of $CrAlN_R$ film: **a)** SEM cross-section observation at 3.5% of Al, **b)** top surface at 3.5% of Al, **c)** and detail **d)** HRTEM picture of CrAlN film clearly showing an amorphous/crystalline nanocomposite micro-structure at 3.5% of Al, and (E) Three-dimensional AFM surface morphologies of $CrAlN_R$ coatings at 3.5% and 24% of Al.

Overall, during this study by AFM, the variability of the RMS roughness as a function of the bias voltage of the substrate (i.e., the power applied to the target) shows a proportionality. This increase in surface roughness is due to an increase in atomic motion and coating densification due to the increased flow and ions energy. Moreover, structural densification and grain development may increase the surface roughness [40]. In fact, the increase in the polarization voltage generates a high mobility of the adatoms and subsequently a nucleation density (Figure 4c,e). Additionally, under high-energy ion bombardment, highly mobile adatoms can diffuse into inter-grain voids, making the film more compact and denser [42]. High levels of Argon ion bombardment at a higher bias voltage also tend to improve etching and result in a smoother surface [43,44]. This has been demonstrated for high proportions of aluminum, such as CrAlNs with 28% of Al and CrAlNR with 24% of Al, which can benefit from high-energy bombardment [45].

The previous descriptions are based on thermodynamic equilibrium assumptions. To better understand the growth of the coating, one must look at the elementary processes at the atomic level. The species resulting from the incident flow are adsorbed and can also be desorbed. The desorption being thermodynamically activated is negligible for the metals which are deposited at moderate room temperature. If the atoms remained at the impact site, the fluctuation of the incident flux would result in faster increasing roughness.

We could model this growth as non-interacting atomic columns subjected to a Poisson-type particle flow. The roughness would be the standard deviation of this distribution, which is proportional to the square root of the thickness [38]. However, surface atomic diffusion (adsorbed atoms) ensures the redistribution of atoms. The diffusion of adsorbed atoms is much easier than volume diffusion (lower activation energy), and even at room temperature, it is active for metals. However, there are mechanisms that hinder the surface-smoothing effect of diffusion for adsorbed atoms. These hindrances are associated with the inherent characteristics of the crystal lattice, such as the adsorption of atoms in crystal lattice gaps or the formation of stable islands of a certain size. The movement of adsorbed atoms can occur through upward or downward diffusion, establishing mechanisms for their mobility.

3.1.3. XRD analyses of the CrAlN layers

Figure 6 shows the diffractograms of $CrAlN_s$ films for different Al percentages as well as of the silicon substrate. The latter has been added to facilitate the identification of peaks by focusing only on those corresponding to the layers and not on the substrate. On the diffractogram of the CrN layer (0% Al), there is a large peak exhibiting almost amorphous layer. This peak is perhaps the result of the contribution of several others such as: the Cr_2N (111) observed at 50.42 °, Cr_2N (200) observed at 50.58° from the hexagonal phase Cr_2N (hcp), and CrN (200) observed at 51.20° from the face-centered cubic phase of CrN (fcc). The EDS analyzes of this film give a Cr/N ratio of 2.5, which suggests that under these deposition conditions Cr_2N is obtained instead of CrN or a two-phase mixture.

According to the previous results, Al addition improves the crystallization of the $CrAlN_s$ layers and promotes the formation of different crystalline phases. Indeed, several peaks were observed in the case of cubic CrN (c-CrN (110) at 43.58° and (200) at 51.20°), hexagonal Cr_2N (h-Cr_2N (110) at 44.15°, (111) at 50.42° and (200) at 50.58°), cubic AlN (c-AlN (111) at 45.05°, (200) at 52.49 ° and (400) at 53.71°) and hexagonal AlN (h-AlN (002) at 42.10° and (101) at 44.45°). Comparable results have been obtained in other studies [42]. A translation of these peaks towards the large angles has been visualized, which shows that CrAlNs films contain compressive stresses, a result already found in other studies [43]. At 24% Al, a single AlN (101) peak is present at 44.45°. This peak disappears at 51% Al to give way to a large AlN (002) peak detected at 42.10°, and the CrAlN films become again

Preprints (www.preprints.org) | NOT PEER-REVIEWED | Posted: 10 July 2023 doi:10.20944/preprints202307.0562.v1

amorphous. These last two peaks relate to the hexagonal AlN phase (hcp), which shows that there has been a crystal change from a cubic phase (C-AlN) to a hexagonal phase (H-AlN).

Moreover, equilibrium diagrams of Cr-N and Al-N [42] showed that the formation of C-CrN and C-AlN is only possible at 50% nitrogen. However, according to AFM analyzes (Figure 5), the nitrogen content in the CrAlN layers varies between 28 and 33%. These low nitrogen contents would allow the formation of hexagonal Cr_2N and AlN instead of cubic CrN and AlN. It is consequently probable that our layers are in the form of multiphases where we have the formation of cubic CrN and AlN when the stoichiometric ratios Cr/N and Al/N are close to 1. But if these ratios are close to 2, the hexagonal Cr_2N phases and AlN form.

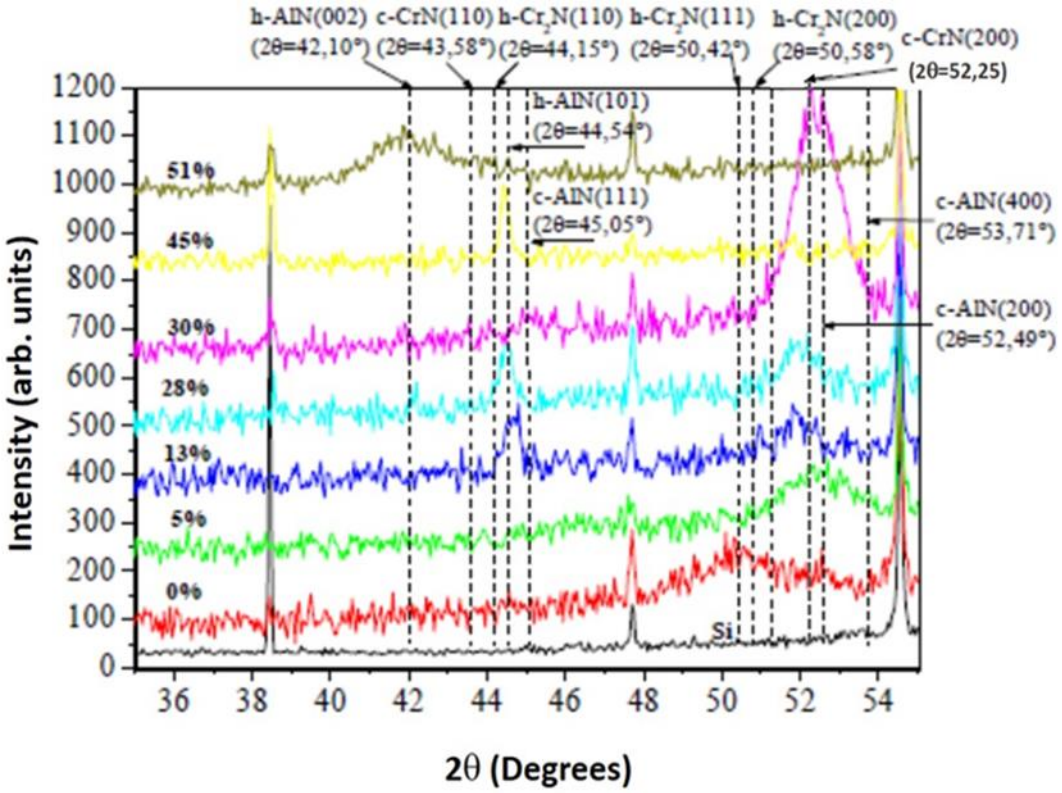

Figure 6. XRD patterns of $CrAlN_S$.

Figure 6 shows the diffractograms of $CrAlN_R$ films with different Al contents (Variation of the target power). All films show the AlN (101), CrN (200) and CrN (202) peaks. For a small amount of Al (3.5%), the cubic phase peak of AlN (101) is identified at the angle of 43.8°. The CrN (200) and CrN (202) phases are also detected at the angles 51.5° and 75.04°. The AlN (101) peak is broad with low intensity. This may be due to the low amount of Al and therefore low crystallinity. The CrN peak (200) is shifted towards the large angles. This shows that $CrAlN_R$ films exhibit residual compressive stresses. By increasing the percentage of Al to 7%, the intensity of the AlN (101) phases increases. This good crystallinity is probably attributed to the J_{ion}/J_{atom} ratio with J_{ion} the ionic flux density and J_{atom} the flux density of atoms during layer growth [43]. According to Wang [45], this ratio is proportional to the I_b/R_b ratio where I_b is the bias current of the substrate during deposition and R_b is the deposition rate. They have shown that this ratio increases with the I_{Al}/I_{Cr} ratio. This increase in ion bombardment and the resulting improvement in ad-atom mobility are beneficial for the development of the crystalline phase of CrN (200). In addition, with the increasing low-energy ion bombardment, defects are reduced, and a denser microstructure is developed. Therefore, the crystallinity of CrAlN films improves with increasing Al content (or target Al flux) at low Al/Cr ratio values. However, as the Al content increases, the distortion of the lattice becomes larger due to the substitution of the Cr atoms by the smaller Al atoms. This results in a decrease in crystallinity. As the percentage of Al in the layer increases from 3.5% to 24%, so the intensity of the AlN (101) phases

Preprints (www.preprints.org) | NOT PEER-REVIEWED | Posted: 10 July 2023 doi:10.20944/preprints202307.0562.v1

increases. This improvement in the crystallinity of $CrAlN_R$ films with an Al content of 19 and 24% is explained by the increase in the crystallization rate [44]. Indeed, the particle size of the $CrAlN_R$ film with an Al content of 11% is about 38 nm. For an Al level of 24% in the layer, the size increases to 77 nm (Figure 6). This result of grain size increase for a high bias voltage is already confirmed by AFM analysis (Figure 5).

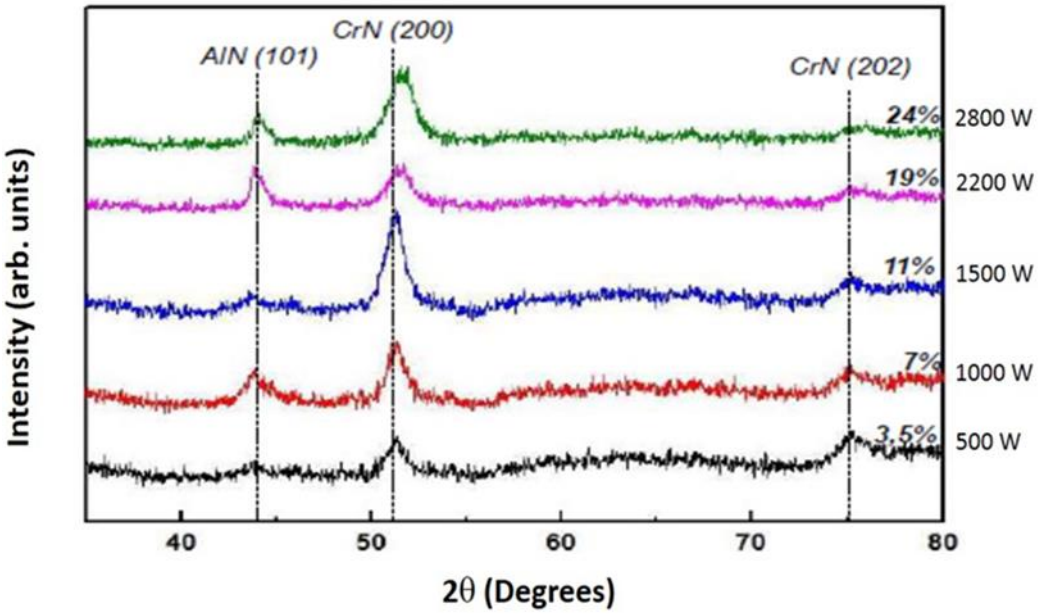

Figure 7. XRD patterns of $CrAlN_R$.

Following various analyzes carried out by DRX on $CrAlN_S$ and $CrAlN_R$, we deduce that neither the growth nor the phases are similar. In fact, the impact of the rotation affects the morphology, the structure, the phases and even the composition of the coating. The increase in the proportion of aluminum does not lead to a further increase in the N content. At this stage, the CrAlN films are not saturated (N/(Al + Cr) <1); that is, the material properties of $CrAlN_R$ films are like those of a partially nitride coated film. The Al/(Al+Cr) ratio is maintained at values below 0.5, which favor the formation of the h-AlN (101) phase in the CrAlNs films. It should be noted that the oxygen content of all films is less than 0.5%.

When Cr is mixed with AlN, the larger Cr atoms partially occupy the Al sites to form a solid solution of CrAlN, thus changing the lattice parameters as follows: CrN (0.41480 nm) and AlN (0.4045 nm) [45]. It should be noted that the hexagonal structure characteristic of AlN crystals appears in the two CrAlN films (rotating and stable substrates), due to the low ratio (Al / (Al + Cr)) <0.5; that is, below the critical point at which AlN would form. At 30% Al (CrAlNs) content, a broad peak appears due to the appearance of c-CrN (200) and c-AlN (200), with the mixture of a dense and well crystallized structure.

3.2. Mechanical properties and corrosion

3.2.1. Internal stresses of the CrAlN layers

The measurements of the residual stresses of CrAlN coatings as a function of the proportion of aluminum are presented in Figure 8. The CrAlNs deposited thin films have compressive stresses which vary between -1 and -3.5 GPa (Figure 8a). The work of Wang et al. [45] showed comparable results. As depicted in Figure 8a, the residual stress reaches its maximum value at an Al content of 30%, after which the values decrease. In contrast, the residual stress in CrAlNR films does not exceed -0.125 GPa and is accompanied by a positive value for a 0% Al proportion (Figure 8b). Nouveau et al. [48] also obtained similar results on CrN and Cr2N layers, showing that the spherical grains of thin layers (<250 nm) transform into elliptical grains as the layer thickness increases (>250 nm). This

Preprints (www.preprints.org) | NOT PEER-REVIEWED | Posted: 10 July 2023 doi:10.20944/preprints202307.0562.v1

behavior is attributed to the difference in growth rate of the crystallite planes, with grains having a low surface energy growing preferentially over grains with a higher surface energy. Additionally, Nouveau et al. [48] hypothesized that internal stresses, caused by the accumulation of crystal defects during deposition, can lead to stress reduction through complete recrystallization of the film.

Therefore, we can divide this growth pattern into three stages:

Step 1: At the start of growth, the nucleation of small crystallites only appears after formation of an amorphous layer of 3 to 10 nm thick. In the case of CrAlN layers, these crystallites are oriented along the densest planes. This step is characterized by a somewhat high densification and stress level.

Step 2: When the layers reach thicknesses of the order of 150 nm, a change in the growth mode of these layers is observed. Indeed, the layer is then subjected to significant constraints (almost non-existent empty spaces) and will have to adapt to be able to grow. For this, it will continue the columnar growth but in such a way that there will be formation of conical columns. This new growth will favor the previously most developed columns governed by shadow effects which will induce new inter-column spaces and therefore weaker constraints.

Step 3: beyond this thickness, we arrive at the stabilization of the level of stresses and density; it is the state of equilibrium. The effect of ion bombardment remains negligible due to the growth of the columnar structure which justifies the stability of the stresses over the entire thickness.

We can therefore think that the layer changes its mode of growth under the effect of too strong constraints in order not to delaminate and continue its thickening.

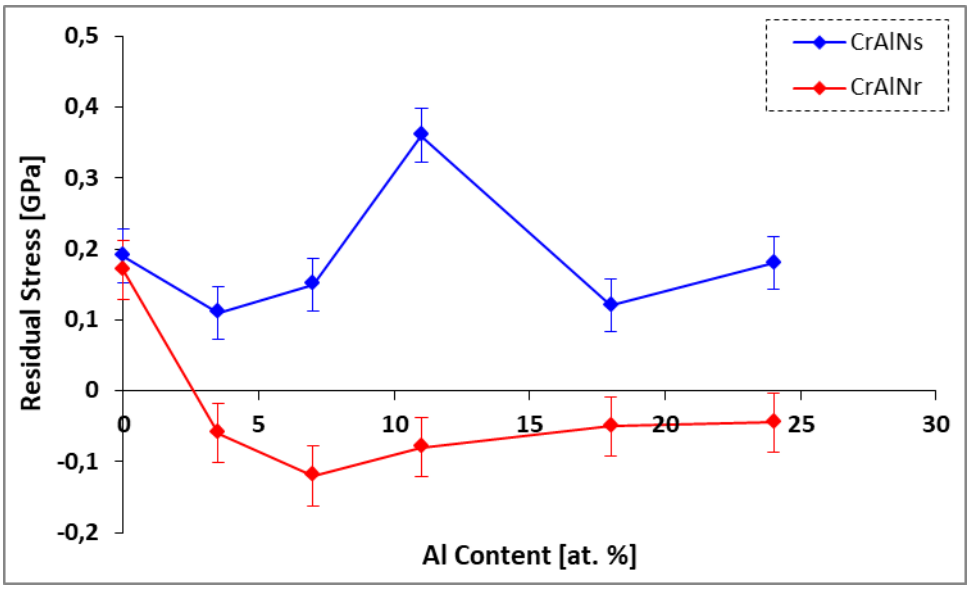

Figure 8. Residual stresses determined by 2D profilometry and the Newton's ring method vs the Al content in the CrAlN films for $CrAlN_S$ and $CrAlN_R$ modes deposed.

In conclusion, the $CrAlN_S$ and $CrAlN_R$ layers exhibit compressive stresses. If we compare the stresses of the two layers obtained under similar deposition conditions (120 min, 0.5 Pa, 3.5% Al for $CrAlN_R$ and 5% Al for $CrAlN_S$ and about 20–25% nitrogen in the plasma), they are of the order of -2 GPa ($CrAlN_S$) and -0.075 GPa ($CrAlN_R$) which is quite different. This difference is strongly linked to the rotation of the substrate, which is responsible for the development of elementary defects in the structure of the $CrAlN_R$ coating. In addition, varying the target/substrate distance results in a loss of energy from the atoms. The coupling of different phenomena leads to a decrease in the level of internal stresses in the $CrAlN_R$ coating.

Based on various experimental studies, it has been deduced that the rate of crystallization in CrAlNS layers results in a higher density compared to that in CrAlNR layers. The rotation of the substrate creates more defects and distortions in the crystal lattices, leading to a relaxation of the internal stresses in the CrAlNR coatings. In contrast, the stationary $CrAlN_S$ substrates are

Preprints (www.preprints.org) | NOT PEER-REVIEWED | Posted: 10 July 2023 doi:10.20944/preprints202307.0562.v1

accompanied by higher internal compressive stresses than CrAlNR, this is the effect of the growth of dense coatings, with fewer defects.

3.2.2. Hardness, Young's modulus, friction coefficient and wear of the CrAlN films

3.2.2.1. Hardness, Young's modulus of the CrAlN films

To determine the hardness of the layers, nano-indentation tests were carried out on CrAlN films deposited on 90MnCrV8 steel substrates. The hardness values are determined using the Rahmoun model [34]. Figure 8 shows the effect of changing the percentage of Al in the layer on its hardness. The mechanical properties of CrAlNS coatings as a function of the voltage of the Cr and Al targets are shown in Figure 8a. The measurements obtained show values of the order of 20 to 40 GPa for the hardness and from 360 to 465 GPa for the Young's modulus. Comparable values have already been obtained in previous studies [43–45]. The evolution of hardness and Young's modulus showed a peak (maximum) for 30% Al content. This may be due to the formation of a solid solution originating from a substitution of chromium atoms [41]. The average values of hardness and Young's modulus is 30 GPa and 420 GPa, respectively. To explain the obtained values, two phenomena can be highlighted since they can impact these measurement values: one is the formation of a solid solution and the other is the number of defects created during the deposition process.

In contrast, for CrAlNR coatings, adding 3.5% of Al in the films increases the hardness from 22 to 28 GPa. This improvement in hardness can be attributed to the short interatomic distance and increases of density in the CrAlN films [43]. In addition, the strong stresses induced inside the mesh reinforce the structure and make it rigid, which leads to an increase in hardness. By increasing the percentage of aluminum in the layer to 11%, the hardness and the Young's modulus decrease slightly and reach 24 GPa and 287 GPa respectively. This can be explained by the relaxation of the residual stresses (Figure 9b). For Al contents of 19 and 24% in the layer, the hardness and Young's modulus is maximum and reach respectively 30 and 347 GPa for 24% of Al. This is attributed to the formation of a solid solution which results from the substitution of Cr atoms by Al atoms [40–42].

The comparison of the mechanical properties of two production methods of the CrAlN coating shows that the rotation of the substrate reduced the hardness and the Young's modulus by approximately 10 to 15% compared to the stationary substrate. On the other hand, the advantage of the rotation of the substrate is to obtain a homogeneous structure which limits the dispersion on the measurements. Therefore, the hardness changes from a value between 20 and 40 GPa obtained on CrAlNS (Figure 9a) to another value between 18 and 32 GPa on CrAlNR (Figure 9b).

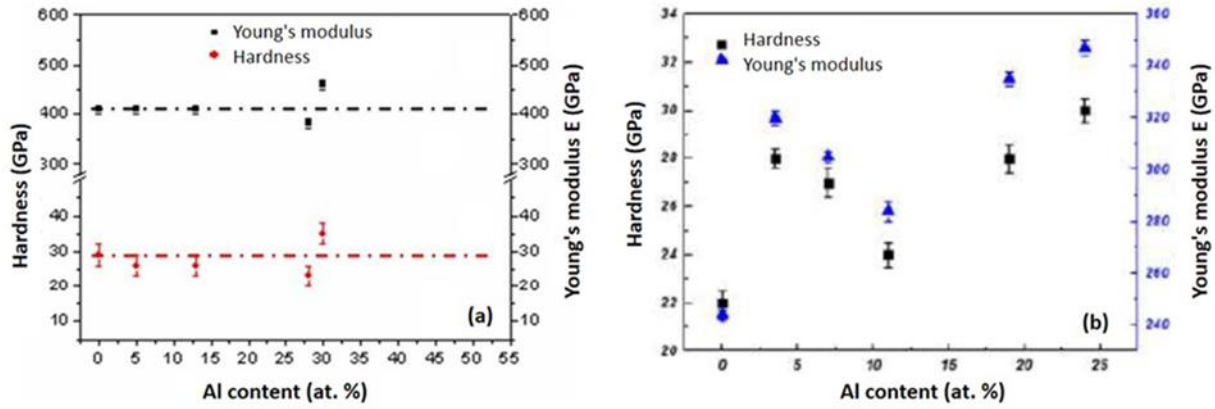

Figure 9. Microhardness and Young's modulus profiles as a function of Al element concentration for the two deposition modes: **a)** CrAlNS and **b)** CrAlNR.

3.2.2.2. Adhesion strength prediction of CrAlN coatings

Figure 10 presents the results of the adhesive strength measurement (Lc) of CrAlNR and CrAlNS coatings. The adhesive strength values exhibit a peak for both modes (CrAlNR and CrAlNS) of the

Preprints (www.preprints.org) | NOT PEER-REVIEWED | Posted: 10 July 2023 doi:10.20944/preprints202307.0562.v1

coatings deposited on the 90CrMoV8 steel substrate. The initiation of cracks and wear debris can be detected after certain sliding distances during friction-wear tests. The initiation appears to be delayed for the rotating mode and dependent on the aluminum content, while at higher percentages of Al, the stationary or rotating mode no longer has an impact on the adhesion of the coating layers. This variation is likely related to residual stresses in the CrAlN coating. In fact, the higher the tensile residual stresses, the lower the adhesion. Thus, samples with lower compressive residual stresses exhibit better adhesion than those with higher tensile stresses.

Indeed, according to Kim and Lee [48], Figure 9 shows that the addition of Al decreases the residual stress, which may explain the increase in Lc at -300 V (5% Al) applied to the Al target. Then the stress increases slightly to -500 (13%) and -700 V (28% Al), applied to the Al target, and therefore Lc decreases. At -900 V (30% Al), we obtained the least adhesive coating because the residual stresses in this coating are tensile and maximum. For the two films obtained at -700 (45%) and -500 V (51% Al) Lc increases considerably because their respective residual stresses decrease. For all Scratch-Tests, the CrAlNR coating exhibits better adhesion than its CrAlNS counterpart.

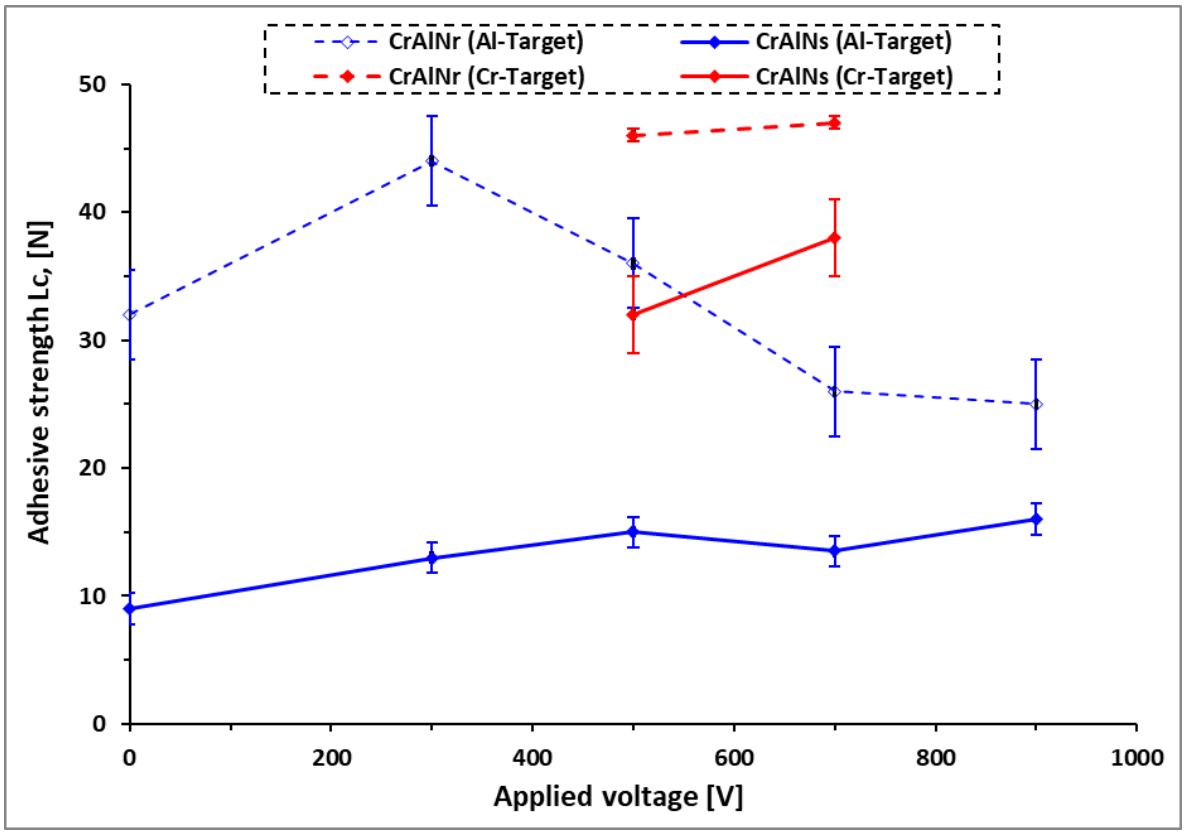

Figure 10. Friction coefficient of CrAlN films: a) CrAlNS films and b) CrAlNR films.

3.2.2.3. Friction coefficient of the CrAlN films

The coefficient of friction of the CrAlN layers during stabilization is between 0.65 and 0.8 (Figure 11a,b) with a voltage applied to the aluminum target (0 to -900 V for CrAlNS) or power of the Al target (0 to 2800 W for CrAlNR). Comparable values have been found in previous studies [33]. According to Bobzin et al. [22], AlN layers have a higher coefficient of friction than CrN and CrAlN layers, so we can say that the presence of c-AlN and h-AlN phases are responsible for the high coefficient of friction. However, these values of the friction coefficient before the appearance of the damage of the coating are lower than that of the substrate which should be close to 1. Furthermore, Tian et al. [39] explained the increase in the friction coefficient of CrAlN films compared to that of CrN by the increased resistance to oxidation. They consider that the oxide layer formed in the CrN film acts as a lubricant due to its low shear strength, resulting in a low coefficient of friction. With the

Preprints (www.preprints.org) | NOT PEER-REVIEWED | Posted: 10 July 2023 doi:10.20944/preprints202307.0562.v1

incorporation of a small amount of Al, the oxidation behavior improves. Therefore, the lubricating effect of the oxide layer is reduced, which may explain the increase in the coefficient of friction.

For CrAlN$_R$ coatings, by adding a proportion of Al between 7 and 24%, the coefficient of friction is almost stable (around 0.8) and the change in the level of Al has no influence on it. Similar results were found by Chim et al. [1]. This stability of the coefficient of friction is probably attributed to the fact that the intensity of the AlN phase remains unchanged. The comparison of the two curves of Figure 10 shows that the friction distance before the appearance of cracks and wear on the coatings is improved in the case of the rotating substrate (CrAlN$_R$). Considering the proportions of aluminum in the CrAlN coating, the friction distance without the appearance of any type of failure is between 20 and 45m for CrAlN$_S$ (Figure 11a) and between 40 and 60m for CrAlN$_R$ (Figure 11b). Consequently, the presence of the AlN phases has a poor effect on the tribological behavior of CrAlN$_S$, and the coefficient of friction is sensitive to the intensity of the AlN phases and not only to their existence as a basic constituent of the CrAlN layer.

In general, the results of this experimental study indicate that the rotation of the substrate has an impact on the structural and microstructural characteristics and properties of the CrAlN coating. The rotation of the substrate results in a CrAlN$_R$ coating of columnar structure accompanied by a random orientation, thus the hardness and the coating-substrate adhesion are relatively low. On the other hand, for a stationary substrate, the CrAlN$_S$ coating exhibits a strong texture of the privileged direction (200), accompanied by a dense and equiaxial grain structure. Conversely, the hardness and adhesion of coatings (CrAlNS) on an immobile substrate are higher than those deposited on rotating substrates. The phenomena observed in CrAlN coatings are believed to be related to the energy of the atomized flux, which is linked to the substrate-target distance during deposition.

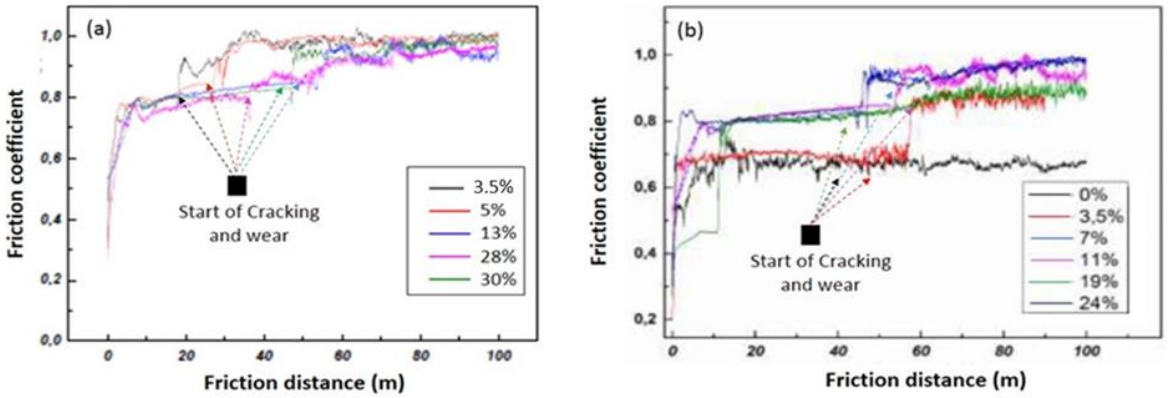

Figure 11. Wear volume of the different substrates after a sliding distance of 40m, Fn =1N, T= 22 °C and 0.01ms^{-1} circumference velocity, with **a)** CrAlN$_S$ and **b)** CrAlN$_R$.

3.2.2.4. The wear mechanism of CrAlN films

Figure 12 represents the used volume for the two types of coatings (CrAlNS and CrAlNR). The increase in the percentage of Al in the diaper is accompanied by an increase in the volume of wear. This change in wear volume is related to the decrease in hardness, adhesion, and density of the microstructure. This is because the wear resistance increases with hardness and adhesion. Based on the two curves, the rotation of the substrate has a detrimental effect on the wear resistance of the CrAlN coating. In fact, the wear volume on CrAlNR is higher than that on CrAlNS. On the one hand, this difference is linked to the crystalline structure (semi-crystalline) and to the good adhesion of CrAlNs to the substrate. On the other hand, this result is probably attributed to the energy dissipated by friction of the antagonists in contact. This is consistent with the work of Tian et al. [39].

Preprints (www.preprints.org) | NOT PEER-REVIEWED | Posted: 10 July 2023 doi:10.20944/preprints202307.0562.v1

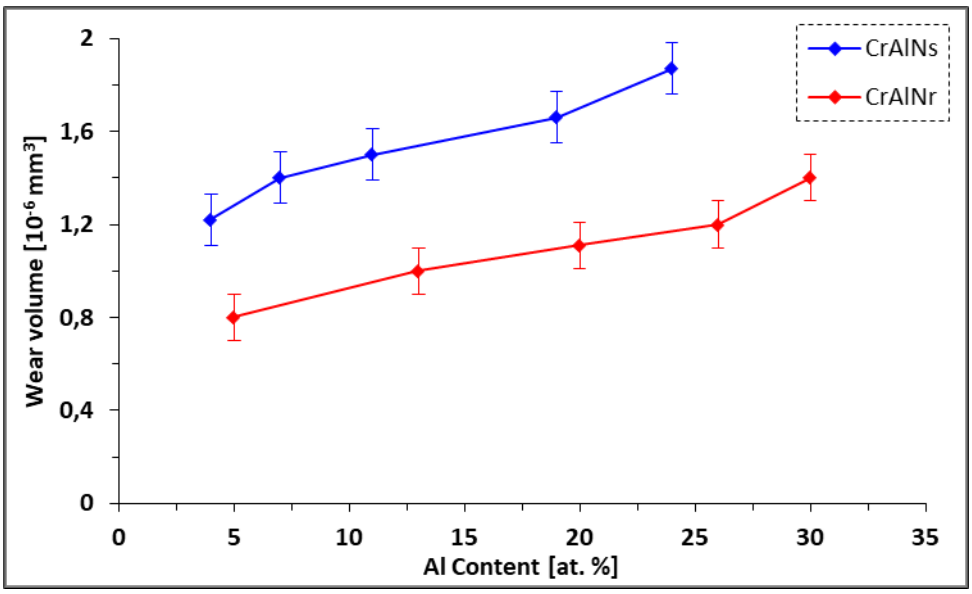

Figure 12. SEM images and EDS analyze of chemical elements in the wear tracks of **CrAlN**$_S$ coatings (with different % Al) deposited on 90MnCrV8.

To study the wear mechanism on CrAlN$_S$ and CrAlN$_R$ coatings, the wear marks are observed by SEM and completed by EDS analyzes (Figure 13). In general, after the wear tests, a high level of oxide is obtained. This indicates the existence of a local high temperature in the contact zone between the antagonists in contact (ball/sample). For the CrAlN$_S$ film, we observe the presence of a significant amount of chromium, aluminum, and nitrogen in the wear trace, which proves the existence of the CrAlNs layer. On the other hand, the amount of iron is very low, which shows that the alumina bead does not completely rub on the base substrate (Figure 13). For the CrAlN$_R$ coating, the presence of a significant amount of molybdenum (Mo) and iron is observed after the friction tests. This proves that the CrAlN$_R$ layer is partially removed. The wear is manifested at the level of the friction trace of the CrAlN$_R$ films by cracking and partial chipping in the trace. These results may inform us about the adhesion of CrAlN$_R$ and CrAlN$_S$ films. We can conclude that the CrAlN$_S$ coating has better adhesion than CrAlN$_R$, which is consistent with the tribological behavior of the coatings studied previously. In fact, good tribological behavior is combined with good wear resistance.

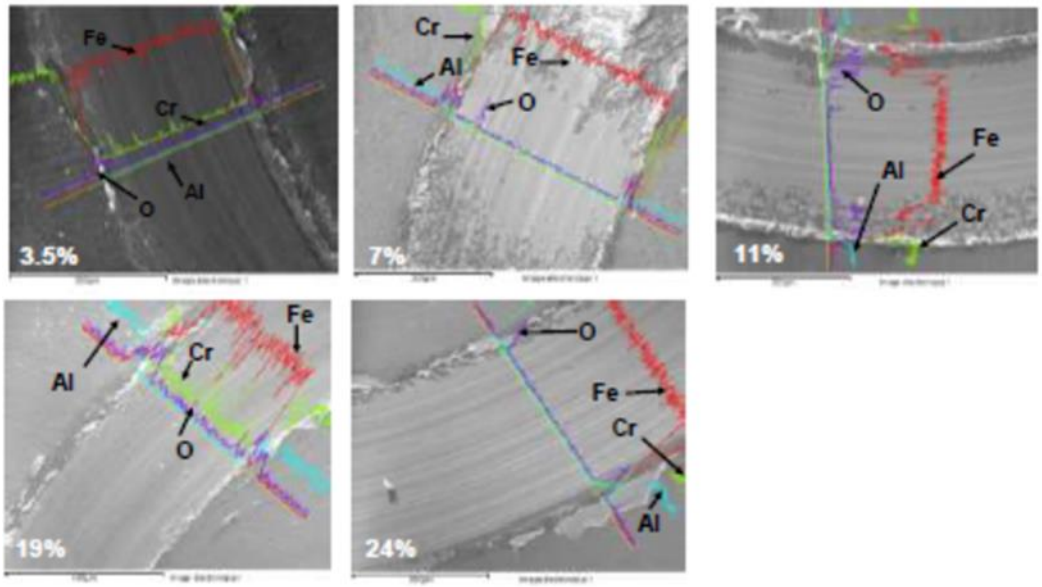

Figure 13. SEM images and EDS analyzes of chemical elements in the wear tracks of **CrAlN**$_R$ coatings (with different % Al) deposited on 90MnCrV8.

 doi:10.20944/preprints202307.0562.v1

3.2.3. Electrochemical tests

It is well known that the corrosion properties of the layers depend largely on their microstructure. Generally, hard coatings produced by PVD are known by their columnar structure. This structure results in straight grain boundaries with open pores which provide efficient diffusion channels for the penetration of corrosive electrolytes into the substrate. By incorporating Al atoms into the Cr-N binary system, the coating structure becomes finer, sometimes accompanied by the formation of nano-layers at the coating/substrate interface (Figure 4a). This structure changes the direction of corrosion, from one vertical propagation to another transverse, which slows down the corrosion rate and therefore the attack on the substrate. Mani & al. [40] mentioned that the corrosion resistance of monolayer coatings is mainly linked to the deflection and arrests the propagation of microcracks and dislocations at the interface of the superimposed layers. This phenomenon is also coupled with the prevention of the continuity of pinholes/pores.

Thus, the crystallite boundaries become discontinuous in the structure (Figure 5a). This decreases the likelihood of having blemishes through the porosity, pitting, droplets and other growth defects formed during the PVD deposition process. Thus, the diffusion of corrosive reagents must follow a zigzag path which slows down the corrosion process and makes it difficult. As a result, the corrosion resistance improves. However, with increasing Al content in CrAlN films, roughness increases (Figures 5c and 4c). This results in an increase in the number of coating defects which has the consequence of reducing the corrosion resistance of the system. Therefore, the rougher the surface, the higher the number of defects. According to Figure 14, the surface of the CrAlN film with the following proportions of aluminum 28% (for $CrAlN_S$) (Figure 14a) and 7% (for $CrAlN_R$) (Figure 14b) has the lowest surface roughness. This explains its better resistance to corrosion. In general, the $CrAlN_S$ coating has better corrosion resistance than its $CrAlN_R$ counterpart.

This good corrosion behavior is probably associated with the density of the microstructure of this $CrAlN_S$ layer (Figure 14a). In fact, this coating has fewer defects compared to the $CrAlN_R$ layer. Generally, atoms in areas with defects have a very high free chemical energy than that of atoms in closed areas [44]. These atoms can react with the active particles in the corrosive solution, producing a zone of surface corrosion. On the other hand, the corrosion phenomenon is initiated rapidly in the pores present on the surface of the coating due to its small thickness [43], which accelerates the rate of corrosion. In addition, the good corrosion behavior may be due to the better properties of this thin films such as its roughness and its adhesion. In principle, cracks and grain boundaries provide preferential channels for corrosive agents that can reach the substrate [38]. Likewise, grain size can affect corrosion resistance. Indeed, the corrosion resistance improves with the decreasing grain size [35], which is consistent with Figure 14a. Through the various experimental investigations, we can conclude that the variation of % Al does not affect the corrosion resistance of the $CrAlN_R$ coatings too much (Figure 14b). The rotation of the substrate has a significant impact on the homogeneity of the electrochemical properties of the layer. This contrasts with CrAlNS coatings, which exhibit heterogeneity, particularly for high aluminum proportions (28% to 30% Al).

Referring to the polarization curve, we notice the existence of two zones (Figure 14a). At the start of the anode zone (zone 1), we observe that the oxygen diffusion level for all the thin films is almost the same except that of 28% Al, which is almost linear. This film therefore protects the surface of the thin films by reducing the corrosion current density. Thus, this film acts on the corrosion kinetics. Indeed, because this film has fewer pores than the other coatings, their plugging with the oxide will be easier and faster. Also, at the end of the cathode zone (zone 2), we observe the existence of a pitting potential for the film produced in a proportion of 28% Al. This phenomenon results in the breakdown of the oxide layer by Cl^-. Similarly, this phenomenon can be created by the presence of inclusions on the surface.

Preprints (www.preprints.org) | NOT PEER-REVIEWED | Posted: 10 July 2023 doi:10.20944/preprints202307.0562.v1

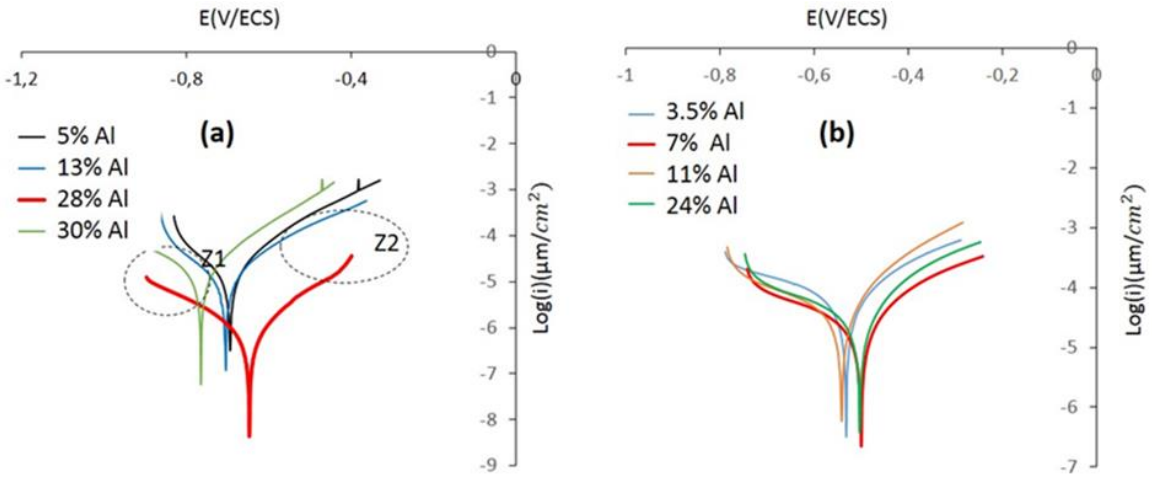

Figure 14. Potentiodynamic polarization curves (Tafel curves) of the different layer coatings in a 3% NaCl aqueous solution: a) CrAlN$_S$ films and b) CrAlN$_R$ films.

4. Conclusions

The aim of this work is to validate the usefulness of CrAlN coatings in different deposition modes (stationary and rotary) on 90CrMnV8 steel substrates. The intended industrial application is to make this steel grade suitable for the manufacture of hot-forming press tools. The criteria for choosing one mode or another are based on functional performance in service, such as wear resistance, friction and corrosion resistance. Surface properties (microhardness, structure, residual stresses) were examined to qualify the coating layers thus established. The main results expected for CrAlN layers obtained by DC magnetron sputtering are listed in the following points:

a) EDS analyses confirm that the structure of the CrAlN layers is a solid solution allowing the substitution of Cr atoms by Al atoms, showing that the sensitivity constant is more stabilized on CrAlN$_R$ films than on CrAlN$_S$, reflecting the impact of the substrate's rotational mode on film homogeneity.

b) Both CrAlN$_S$ and CrAlN$_R$ films are well crystallized at low aluminum content. At higher aluminum contents, CrAlNS films become amorphous. In addition, the CrAlNR coating is composed of two phases (CrN and AlN) for the rotating substrate and three phases (Cr_2N, CrN and AlN) for the stationary substrate.

c) CrAlN$_S$ coatings exhibit tensile stresses, while CrAlNR has generated residual compressive stresses. Indeed, substrate rotation generates relaxation of internal coating stresses (defects, high target ionization rate), also accompanied by low density.

d) CrAlN$_R$ films have better tribological properties than the CrAlN$_S$ case, although the maximum values of the coefficient of friction are comparable (around 0.8). However, the friction distance (without the appearance of defects) on CrAlN$_R$ is longer than on CrAlN$_S$. This is because the presence of the c-AlN and h-AlN phases has a detrimental effect on the coefficient of friction, and subsequently on the rapid degradation of CrAlNS coatings.

e) The deposition under optimum conditions yielded maximum hardness and Young's modulus values of 40 GPa and 465 GPa, respectively, for the CrAlNS films. In contrast, the CrAlNR layers achieved slightly lower values of 32-33 GPa and 350-352 GPa, respectively.

f) We conclude that the CrAlN$_S$ and CrAlN$_R$ coating systems have optimal electrochemical behavior, for the 28% Al and 7% Al properties respectively. The density of growth defects (effect of aluminum incorporation and substrate rotation) has a more significant effect on corrosion behavior than other properties, such as: micro-structure, wear and tribological properties.

Acknowledgments: The authors would like to thank the Regional Council of Burgundy for its financial support. The authors also would like to thank M. Denis LAGADRILLERE for the SEM observations and EDS microanalyses, and Dr. Philippe JACQUET for the XRD analyses. We also thank Pr. Alain IOST and Dr. Alberto MEJIAS for their help in nanoindentation and scratch test measurements.

Conflicts of Interest: The authors declare no conflict of interest.

References

1. Y.C. Chim, X.Z. Ding, X.T. Zeng, S. Zhang. Oxidation resistance of TiN, CrN, TiAlN and CrAlN coatings deposited by lateral rotating cathode arc. Thin Solid Films. 2009, Vol. 517, pp. 4845-4849. https://doi.org/10.1016/j.tsf.2009.03.038.
2. Q. Chen, Y. Cao, Z. Xie, T. Chen, Y. Wan, H. Wang et al. Tribocorrosion behaviors of CrN coating in 3.5wt% NaCl solution. Thin Solid Films. 2017, Vol. 622, pp 41-47. https://doi.org/10.1016/j.tsf.2016.12.023.
3. B. Tlili, C. Nouveau, M.J. Walock, M. Nasri, T. Ghrib. Effect of layer thickness on thermal properties of multilayer thin films produced by PVD. Vacuum. 2012, Vol. 86, pp 1048-1056. https://doi.org/10.1016/j.vacuum.2011.09.008.
4. T. Polcar, T. Kubart, R. Novák, L. Kopecký, P. Široký. Comparison of tribological behaviour of TiN, TiCN and CrN at elevated temperatures. Surface & Coatings Tech. 2005, V193, pp. 192-199. https://doi.org/10.1016/j.surfcoat.2004.07.098.
5. Aouadi, K., Tlili, B., Nouveau, C., Besnard, A., Chafra, M., & Souli, R. (2019). Influence of substrate bias voltage on corrosion and wear behavior of physical vapor deposition CrN coatings. Journal of Materials Engineering and Performance, 28, 2881-2891. https://doi.org/10.1007/s11665-019-04033-y.
6. B. Tlili, N. Mustapha, C. Nouveau, Y. Benlatreche, G. Guillemot, M. Lambertin. Correlation between thermal properties and aluminum fractions in CrAlN layers deposited by PVD technique. Vacuum, 2010, Vol.84, pp. 1067-1074. https://doi.org/10.1016/j.vacuum.2010.01.011.
7. Y. H. Liu, T. Fujita, A. Hirata, S. Li, H. W. Liu, W. Zhang, A. Inoue, and M. W. Chen. Deposition of multicomponent metallic glass films by single-target magnetron sputtering. Intermetallics, 2012, vol. 21, pp. 105–114. https://doi.org/10.1016/j.intermet.2011.10.007.
8. A. Karimi, W. Kalss. Off-axis texture in nanostructured Ti_{1-x} Al_xN thin films. Surface and Coating Technologie. 2008, Vol. 202, 2241-2246. https://doi.org/10.1016/j.surfcoat.2007.08.074.
9. X. Liu, C. Johnson, C. Li, J. Xu, C. Cross. Developing TiAlN coatings for intermediate temperature solid oxide fuel cell interconnect applications. Int. J. Hydrogen Energy, 2008, Vol. 33 189-196. https://doi.org/10.1016/j.ijhydene.2007.09.007.
10. J.L. Mo, M.H. Zhu, B. Lei, Y.X. Leng, N. Huang. Comparison of tribological behaviours of AlCrN and TiAlN coatings deposited by Physical Vapor Deposition, J. Wear, 2007, Volume 263, pp. 1423-1429. https://doi.org/10.1016/j.wear.2007.01.051.
11. J. Yin, R. Hu, X. Shu. Closed-die forging process of copper alloy valve body: finite element simulation and experiments. Journal of Materials Research and Technology, Volume 10, 2021, 1339-1347, https://doi.org/10.1016/j.jmrt.2020.12.087.
12. C. Jácome, C. Angulo, J.C. & Y.A astro. PVD coatings influence (TiCN, BCN, and CrAlN) on the fatigue life behavior of AISI 1045 steel for automotive applications. Int J Adv Manuf Technol **119**, 3995–4009 (2022). https://doi.org/10.1007/s00170-021-08455-8.
13. B.Tlili, C. Nouveau, G. Guillemot, et al. Investigation of the Effect of Residual Stress Gradient on the Wear Behavior of PVD Thin Films. J. of Materi Eng and Perform **27**, 457–470 (2018). https://doi.org/10.1007/s11665-018-3132-1.
14. A.Y. Adesina. Tribological Behavior of TiN/TiAlN, CrN/TiAlN, and CrAlN/TiAlN Coatings at Elevated Temperature. J. of Materi Eng and Perform 31, 6404–6419 (2022). https://doi.org/10.1007/s11665-022-06722-7.
15. W. Tillmann, D. Stangier, B. Denkena et al. Influence of PVD-coating technology and pretreatments on residual stresses for sheet-bulk metal forming tools. J. Prod. Eng. Res. Devel. 10, 2016, 17–24. https://doi.org/10.1007/s11740-015-0653-4.
16. K. Kaouther, D. Hafedh, Z. Lassaad et al. Mechanical Characterization of CrN/CrAlN Multilayer Coatings Deposited by Magnetron Sputtering System. Journal of Materials Eng. and Perform. 24, 2015, 4077–4082. https://doi.org/10.1007/s11665-015-1692-x.
17. Z. Wu, Z. Cheng, H. Zhang, et al. Electrochemical and Tribological Properties of CrAlN, TiAlN, and CrTiN Coatings in Water-Based Cutting Fluid. Journal of Materials Eng. and Perf. 29, 2020, 2153–2163. https://doi.org/10.1007/s11665-020-04772-3.
18. H.N. Shah, R. Jayaganthan. Influence of Al Contents on the Microstructure, Mechanical, and Wear properties of Magnetron Sputtered CrAlN Coatings. J. of Materi Eng and Perform 21, 2012, 2002–2009. https://doi.org/10.1007/s11665-011-0112-0.

19. I. Ebrahimzadeh, F. Ashrafizadeh. A comparative study of surface deformation and quality of brass workpiece in contact with coated dies by pin-on-disc testing. Int. Journal Adv. Manuf. Technology 77, 2015, 609–620. https://doi.org/10.1007/s00170-014-6473-4.
20. W. Shi, Q. Miao, W. Liang, Y. Liu, M. Yin, X. Xu, L. Xue. Gas-solid erosion characteristics of CrAl/CrAlN duplex layer coating deposited by RF magnetron sputtering, Surfaces and Interfaces, Vol. 22, 2021, 100843. https://doi.org/10.1016/j.surfin.2020.100843.
21. C. Li, L. Wang, L. Shang, X. Cao, G. Zhang, & al. Mechanical and high-temperature tribological properties of CrAlN/TiSiN multilayer coating deposited by PVD, Ceramics International, V. 47, Issue 20, 2021, 29285-2929. https://doi.org/10.1016/j.ceramint.2021.07.093.
22. K. Bobzin, C. Kalscheuer, M. Carlet, S. Schmauder, V. Guski, W. Verestek, M. Tayyab. 3D deformation modeling of CrAlN coated tool steel compound during nanoindentation. Surface and Coatings Technology, Volume 453, 2023, 129148, https://doi.org/10.1016/j.surfcoat.2022.129148.
23. E. Haye, F. Deschamps, G. Caldarella, M.L. Piedboeuf, A. Lafort, et al. Formable chromium nitride coatings for proton exchange membrane fuel cell stainless steel bipolar plates. International Journal of Hydrogen Energy, Volume 45, Issue 30, 2020, 15358-15365, https://doi.org/10.1016/j.ijhydene.2020.03.248.
24. S.P. Mani, P. Agilan, M. Kalaiarasan, K. Ravichandran, N. Rajendran, Y. Meng. Effect of multilayer CrN/CrAlN coating on the corrosion and contact resistance behavior of 316L SS bipolar plate for high temperature proton exchange membrane fuel cell. Journal of Materials Science & Technology, Volume 97, 2022, 134-146. https://doi.org/10.1016/j.jmst.2021.04.043.
25. L. Chen, X. Yu. Influence of interfacial structure on the mechanical and thermal properties of CrAlN/ZrN multilayer coatings, Materials & Design, Volume 106, 2016, 1-5. https://doi.org/10.1016/j.matdes.2016.05.082.
26. Evrard, M., Besnard, A. et al. (2019). Study of the influence of the pressure and rotational motion of 3D substrates processed by magnetron sputtering: A comparative study between Monte Carlo modeling and experiments. Surf. & Co.Tech., 378, 125070. https://doi.org/10.1016/j.surfcoat.2019.125070.
27. Kadam, N. R., Karthikeyan, G., & Kulkarni, D. M. (2020). Effect of substrate rotation on the microstructure of 8YSZ thermal barrier coatings by EB-PVD. Materials Today: Proceedings, 28, 678-683. https://doi.org/10.1016/j.matpr.2019.12.276.
28. R. Forsén, M.P. Johansson, M. Odén, N. Ghafoor. Effects of Ti alloying of AlCrN coatings on thermal stability and oxidation resistance. Thin Solid Films, Volume 534, 2013, 394-402, https://doi.org/10.1016/j.tsf.2013.03.003.
29. M. Ahlgren, H. Blomqvist. Influence of bias variation on residual stress and texture in TiAlN PVD coatings. Surface and Coatings Technology. 2005, Vol. 200, pp. 157-160. https://doi.org/10.1016/j.surfcoat.2005.02.078.
30. Wahl, K. J., Chromik, R. R., & Lee, G. Y. (2008). Quantitative in situ measurement of transfer film thickness by a Newton's rings method. Wear, 264(7-8), 731-736. https://doi.org/10.1016/j.wear.2007.04.009.
31. K.D. Bouzakis, N. Michailidis, S. Gerardis, G. Katirtzoglou, & al. Correlation of the impact resistance of variously doped CrAlN PVD coatings with their cutting performance in milling aerospace alloys. Surface and Coatings Technology. 2008. Vol. 203, pp.781-785. https://doi.org/10.1016/j.surfcoat.2008.08.009.
32. Nasser, M., Attyaoui, S., Tlili, B., Montagne, A., Briki, J., & Iost, A. (2021). Identification of Fe-Zn coating behaviors by a new reverse approach using artificial intelligence. Materials Research Express, 8(11), 116401. https://doi.org/10.1088/2053-1591/ac3041.
33. S. Khamseh, M. Nose, T. Kawabata, K. Matsuda, S. Ikeno. Oxidation Resistance of CrAlN Films with Different Microstructures Prepared by Pulsed DC Balanced Magnetron Sputtering System, Mater. Trans., vol. 51, no. 2, p. 271, 2010. http://dx.doi.org/10.2320/matertrans.MC200912.
34. K. Rahmoun, A. Iost, V. Keryvin, G. Guillemot, N.E. Chabane Sari. A multilayer model for describing hardness variations of aged porous silicon low-dielectric-constant thin films. Thin Solid Films, Volume 518, Issue 1, 2009, 213-221, https://doi.org/10.1016/j.tsf.2009.07.040.
35. Beliardouh, N. E., Bouzid, K., Nouveau, C., Tlili, B., & Walock, M. J. (2015). Tribological and electrochemical performances of Cr/CrN and Cr/CrN/CrAlN multilayer coatings deposited by RF magnetron sputtering. Tribology International, 82, 443-452. https://doi.org/10.1016/j.triboint.2014.03.018.
36. L. Wang, G. Zhang, R.J.K. Wood, S.C. Wang, Q. Xue. Fabrication of CrAlN nanocomposite films with high hardness and excellent anti-wear performance for gear applicatio. Surface and Coatings Technology, Vol. 204, Issues 21–22, 2010, 3517-3524, https://doi.org/10.1016/j.surfcoat.2010.04.014.
37. L. Bait, L. Azzouz, N. Madaoui, N. Saoula. Influence of substrate bias voltage on the properties of TiO2 deposited by radio-frequency magnetron sputtering on 304L for biomaterials applications, Applied Surface Science, Volume 395, 2017, 72-77, https://doi.org/10.1016/j.apsusc.2016.07.101.
38. E.C. Romero, M.G. Botero, W. Tillmann, & al. Influence of carbon content on the microstructure, mechanical and tribological properties of CrAlCN coatings deposited by DC unbalanced magnetron sputtering. Bull Mater Sci 41, (2018), 97. https://doi.org/10.1007/s12034-018-1610-6.

39. J.C. S. López A. Contreras S. D. Meister A. G. Luis, M. Brizuela, Tribological behaviour at high temperature of hard CrAlN coatings doped with Y or Zr, Thin Solid Films, Vol. 550, 2014, 413-420. https://doi.org/10.1016/j.tsf.2013.10.041.
40. J. Tian, C. Hu, L.i Chen, Y. Lou, N. Zhao. Structure, mechanical and thermal properties of Y-doped CrAlN coatings. Transactions of Nonferrous Metals Society of China, Vol. 31, Issue 9, 2021, 2740-2749, https://doi.org/10.1016/S1003-6326(21)65689-3.
41. S.P. Mani, P. Agilan, M. Kalaiarasan et al. Effect of multilayer CrN/CrAlN coating on the corrosion and contact resistance behavior of 316 L SS bipolar plate for high temperature proton exchange membrane fuel cell. Journal of Materials Science & Technology, Vol. 97, 2022, 134-146, https://doi.org/10.1016/j.jmst.2021.04.043.
42. B. Xia, S. Zhou, Y. Wang, H. Chen, J. Zhang, B. Qi. Multilayer architecture design to enhance load-bearing capacity and tribological behavior of CrAlN coatings in seawater. Ceramics International, Vol. 47, Issue 19, 2021, 27430-27440. https://doi.org/10.1016/j.ceramint.2021.06.165.
43. A.S. Kuprin, V.D. Ovcharenko, A. Gilewicz, G.N. Tolmachova, & al. Structural, mechanical and tribological properties of Cr-V-N coatings deposited by cathodic arc evaporation. Tribology International, Vol. 165, 2022, 107246. https://doi.org/10.1016/j.triboint.2021.107246.
44. Y. Wang, Ji. Y. Influence of Mo Doping on the Microstructure, Friction, and Wear Properties of CrAlN Films. J. of Materi Eng and Perform 30, 2021, 1938–1944. https://doi.org/10.1007/s11665-021-05557-y.
45. Z. Wang, D. Zhang, P. Ke, X. Liu, A. Wang. Influence of Substrate Negative Bias on Structure and Properties of TiN Coatings Prepared by Hybrid HIPIMS Method. Journal of Materials Science & Technology, Vol. 31, Issue 1, 2015, 37-42. https://doi.org/10.1016/j.jmst.2014.06.002.